Thermochemical Characterization of Materials using a Novel Laser-Heating Technique

Cary Presser[1], Ashot Nazarian[2], and Joseph Conny[3]
National Institute of Standards and Technology, Gaithersburg, MD, 20899

This article reviews the application of a novel rapid laser-heating technique (referred to as the laser-driven thermal reactor) for characterizing multiphase, multicomponent substances. The technique provides quantitative measurements of various relevant thermochemical properties, including sample heat release rate, chemical kinetics rates, total heat value, specific heat release, and chemical reaction byproduct identification. The technique is currently being used to measure the absorption coefficient of particle-coated filters for atmospheric aerosol research. The optical properties of individual particle-laden droplets are also being studied in the laboratory under tropospheric conditions. In addition, a forensic science investigation of energetic materials is underway to develop a database of their thermal and chemical signatures. Past studies include characterization of simulant hazardous organic wastes and propellants for improving storage safety, and planned future studies are to focus on thermochemical characterization of biomass/biofuels/biodiesel. Results presented demonstrate the capability of this technique to address different thermochemical-related issues associated with a wide variety of applications.

I. Introduction

Thermal analysis techniques, such as differential scanning calorimetry (DSC), thermal gravimetric analysis (TGA), and bomb calorimetry are commonly used tools for determining the energy absorption and/or release from materials. In general, they are appropriate for temperature levels up to 1000 K and heating rates up to 1 K/s (limited by instrument design and intended applications). As a result of the limited heating rate (longer time scale), thermochemical phenomena, which potentially can provide important process information, may go undetected by the completion of chemical reactions under investigation. This reduced sensitivity may be attributed, in part, to the limited heating rates available during substance chemical decomposition at higher temperatures. As an example, the literature reports[1] that sodium nitrate ($NaNO_3$) and sodium nitrite ($NaNO_2$) chemically decompose at relatively slow heating rates of 5 K/min at 550 K and 590 K, respectively, but at higher heating rates the rapid temperature rise may lead to an explosion at 810 K. Because of the relatively low heating rate, DSC monitoring of the thermal behavior at higher temperatures may occur after consumption of the chemical reactants, and therefore, fail to detect process features (e.g., exotherms and endotherms). Thus, for this case, higher heating rates are required to appropriately monitor thermal behavior before the occurrence of significant decomposition and completion of chemical reactions. The rapid attainment of high temperatures to diagnose such reactions is achievable with laser-heating techniques.

Several laser-based techniques exist that use high heating rates to determine substance physical properties. For example, laser-induced breakdown spectroscopy (LIBS) and laser induced incandescence (LII) are two such techniques. In LIBS, a focused pulsed Nd:YAG laser is used to rapidly heat metals and form a high-temperature microplasma (on the order of 1×10^4 K).[2] During rapid cooling, radiation is emitted and a spectrometer is used to determine sample composition. Issues include excessive heating effects on changing material properties,[3] and plasma decay rates vary by species so LIBS must be optimized individually.[4] In LII, a pulsed Nd:YAG laser is used to heat soot particles to the carbon vaporization temperature (at about 4×10^3 K). Using thermal energy conservation and the temperature decay time after heating, one may determine the soot primary particle size and volume fraction.[5] Longer decay times are indicative of larger particle sizes.[6] One issue is the effect of laser heating on soot particle morphology and size distribution. More recently, rapid-heating, micro-differential scanning calorimetry[7,8] has been used to heat energetic materials, using a silicon based μ-DSC device (with a heating rate of

[1] Research Engineer, Chemical Sciences Division, 100 Bureau Dr., Mail Stop 8320, AIAA Associate Fellow.
[2] Guest Researcher, Chemical Sciences Division, 100 Bureau Dr., Mail Stop 8320.
[3] Research Chemist, Materials Measurement Science Division, 100 Bureau Dr., Mail Stop 8372.

up to 1 x 10^7 K/s). These devices, however, are limited to small sample quantities, liquid substances, and material temperature.

This article reviews the application of a novel thermal-heating technique, referred to as the laser-driven thermal reactor (LDTR), to multicomponent and multiphase substances. Unlike the aforementioned laser-heating techniques (and respective limitations), the LDTR technique measures the total thermal response (due to both substance thermal and chemical heat release). The technique is used to provide quantitative information on thermochemical properties (e.g., heat capacity, thermal conductivity, emissivity, and absorptivity), chemical processes (i.e., exothermic and endothermic reactions), reaction sequence, and rate constants.

II. Experimental Arrangement

Details describing the LDTR experimental arrangement and theoretical development are published elsewhere,[9-11] with the highlights summarized below. The experimental arrangement consists of a copper reactor sphere (with a diameter of (18.2 ± 0.03) mm and thickness of 0.14 mm) positioned near the center of a 5 L vacuum chamber. The chamber has five viewing ports (four ports on the chamber side placed 90 degrees apart and one port on the top). The top of the vacuum chamber provides access to the reactor. Each viewing port includes a vacuum-sealed 76 mm diameter quartz window, which is suitable for transmission of laser beams to the reactor. Measurements are generally carried out in an inert environment under vacuum to prevent sample oxidation. A schematic of the LDTR reactor sphere and supporting sub-systems is presented in Figs. 1 and 2, respectively.

An opening is in the top of the copper reactor sphere allows for placement of the sample, and another opening in the bottom is used to introduce the thermocouples. Near the center of the reactor sphere, sample is placed on and supported by thin-wire extensions that protrude from near the bead of a thermocouple (see inset in Fig. 1). The reported expanded uncertainties are Type A evaluations (statistical analysis of a series of replicated measurements),[12] which are estimated by determining the standard uncertainty for the variables, completing a propagation of errors analysis, and combining uncertainties to provide the expanded uncertainty. The sample is in contact with a commercially fabricated, K-type, fine-wire thermocouple (0.25 mm in diameter, unsheathed), i.e., 'sample' thermocouple, and a second thermocouple, i.e., 'reactor' thermocouple, is in contact with the reactor inner wall.

Sample is heated indirectly to a preselected steady-state temperature (i.e., the temperature at which the sample is evaluated) by a continuous-wave multi-mode Nd:YAG laser, operating at a wavelength of 1064 nm. The laser light is split into two beams (by directing the light to opposing sides of the reactor surface) and expanded to near the reactor diameter with standard optical components. This laser beam is referred to as the 'heating' beam. Heating to different preselected steady-state temperatures and analyzing the time-resolved temperature measurements (i.e., thermograms) of both the sample and reactor is referred to as the '**heating-rate'** approach. Generally, this approach has been used to obtain chemical kinetic information for chemical reacting processes.

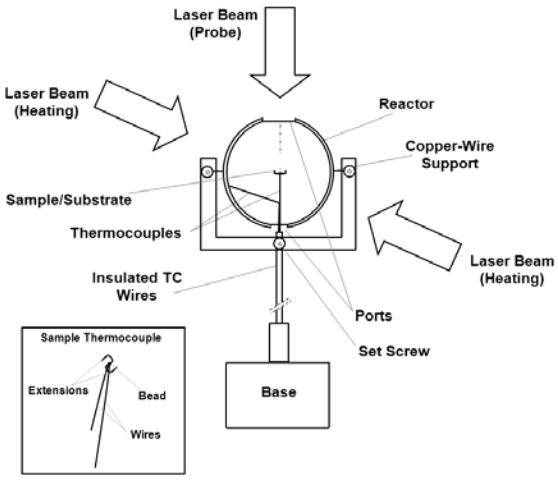

Figure 1. Schematic of the LDTR copper reactor sphere.

Another mode of thermal analysis involves direct laser heating of the sample (after reaching the steady-state temperature) from a third beam of selected wavelength (i.e., the 'probe' beam) down through the opening in the top of the reactor. In our case, this beam is diverted from the heating beam. This mode of operation is referred to as the '**direct-heating'** approach. Thus, at the steady-state sample temperature, the probe beam increases the sample temperature to a new steady-state temperature (of less than 10 % of the initial steady-state value). The temperature decay back to the initial steady-state temperature is then monitored after blocking the probe

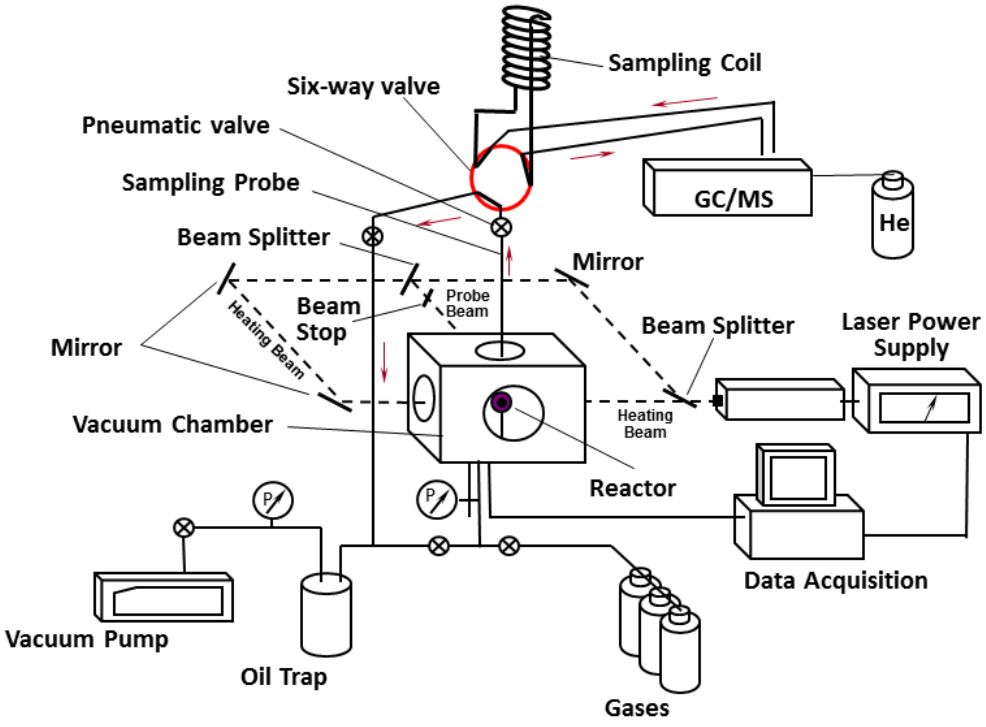

Figure 2. Schematic of the LDTR vacuum chamber and subsystems.

beam. Generally, this approach has been used in nonreacting situations, such as to determine particle absorptivity for filters coated with atmospheric aerosols.

The two approaches have been shown to be equivalent.[9] The use of one approach over another essentially depends on the analysis protocol required to evaluate a particular parameter from the theoretical analysis of the thermal energy conservation equation, as summarized in the next section.

III. Theoretical Development

A. Conservation of Thermal Energy with Chemical Reaction

The theoretical model is based on a representation of the heating process associated with the above-mentioned experimental arrangement. The following thermal energy balance governs the heating process:

$$m(t)\,c_p(T)\,dT/dt = R_1(T_r) - R_2(T) = I_I A\beta(T,\lambda) - F(T,T_o) + \Delta m(t)\,q(T) \qquad (1)$$

where the rate of change of sample internal thermal energy is given by the term on the left side of Eq. 1, $R_1(T_r)$ is the rate at which heat is transferred from the reactor at temperature T_r to the sample, and $R_2(T)$ is the rate of heat loss from the sample, T is the sample temperature, $c_p(T)$ is the sample specific heat capacity at the sample temperature, $m(t)$ is the sample mass with respect to time t. The first term on the right side of the Eq. 1 is the thermal energy absorbed by the sample, where I_I is the laser beam incident radiation intensity that heats the sample, A is the sample geometric cross-sectional area, $\beta(T,\lambda)$ is the sample hemispherical absorptivity at temperature T and laser wavelength λ. The heat transfer term, $F(T,T_o)$, represents the sample thermal energy losses due to conduction, convection, and radiation throughout the arrangement. The parameter T_o is the sample temperature at steady state. Thermal energy losses due to chemical reaction and vaporization are considered if there is a detectable mass change, $\Delta m(t)$, after heating the sample, with $q(T)$ defined as the specific heat release rate due to chemical reactions (i.e., the rate at which thermal energy is released or absorbed by a substance per unit mass during chemical reactions).

B. Analysis Protocol for the Heating-Rate Approach

For the heating-rate approach, an exponentially decaying expression for the rise in temperature to the steady-state temperature is given by:

$$T - T_o = (T_a - T_o)e^{(-t/\tau^*)} \tag{2}$$

This expression is assumed since it fits the experimental data satisfactorily in the regions of interest.[10] The term T_a is the ambient temperature, and τ^* is the temperature-dependent relaxation time. Taking the derivative of Eq. 2 with respect to time results in the expression:

$$dT/dt = -(T - T_o)/\tau^* \tag{3}$$

An analytical expression is derived for τ^* from Eqs. 2 and 3, which is based on obtaining the sample temperature for two different laser fluences (without the reactive sample) from a common value of the reactor temperature, T_r (see Fig. 3A), and is given by:

$$\tau^*(T) = \frac{T_2 - T_1}{\left(\frac{dT}{dt}\right)_1 - \left(\frac{dT}{dt}\right)_2} \tag{4}$$

where T_1 and T_2 are the sample temperatures at time t, and $(dT/dt)_1$ and $(dT/dt)_2$ are the sample temperature-time derivatives (corresponding to T_1 and T_2), for the two different laser fluences, respectively. To compare the sample temperature obtained at the two different heating rates, the reactor temperature must remain unchanged. To accomplish this, a reactor temperature is chosen (with sufficient sensitivity to determine the temperature-time derivatives). Then the two sample temperatures (T_1 and T_2) and corresponding sample temperature derivatives are obtained by extrapolation to the appropriate curves, as illustrated in Fig. 3A. The value of τ^* is determined from Eq. 4 without the sample and thus it is assumed that the thermal energy balance equation for the sample (see Eq. 1) is the sum of a nonreacting and chemical reacting expression. The difference in thermograms with and without sample will be similar, except upon initiation of chemical reactions. This value of τ^* remains unchanged for a particular sample and sample temperature.

C. Determining Substance Total Specific Heat Release

The following protocol is used for cases where one wants to determine the total specific heat release for chemically reacting substances. Once the relaxation time is known, as described above, separate experiments are carried out at a chosen laser fluence for the baseline (no sample) and sample. The equations representing these two experiments are:

with sample

$$m(t)\ c_p(T)\ dT/dt = I_I A\beta(T,\lambda) - F(T,T_o) + \Delta m(t)\ q(T) \tag{5}$$

without sample

$$m(t)\, c_p(T)\ dT/dt = I_I A\beta(T,\lambda) - F(T,T_o) \tag{6}$$

Subtracting Eq. 6 from Eq. 5, substituting into Eq. 4, and rearranging terms results in the following expression for the specific heat release rate, $q(T)$, due to chemical reaction:

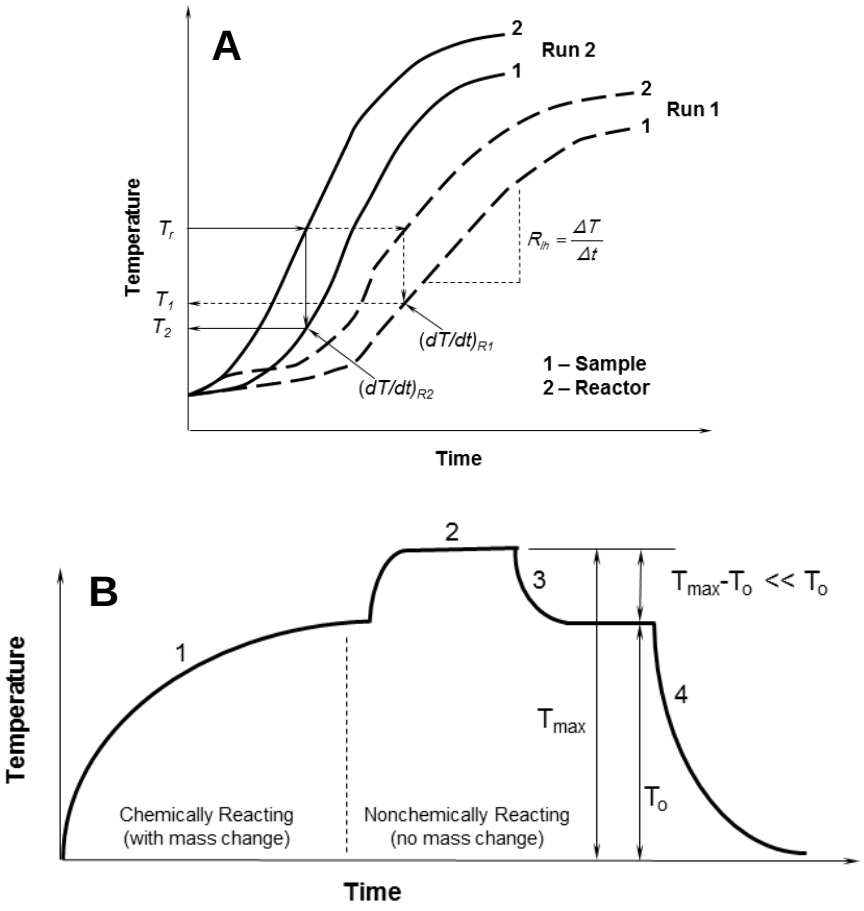

Figure 3. Schematic of the LDTR thermal analysis protocol using the A) heating-rate and B) direct-heating approaches.

$$q(T_s) = \frac{c_p(T_s)m(t)}{\Delta m(t)}\left[\frac{T_s - T_{ws}}{\tau^*} + \left.\frac{dT}{dt}\right|_s - \left.\frac{dT}{dt}\right|_{ws}\right] \tag{7}$$

where the subscript '*s*' refers to the sample in Eq. 5, the subscript '*ws*' refers to without sample in Eq. 6, and all terms can be obtained from the experiment to determine the value of *q(T)*. Integration of Eq. 7 with respect to time (for the entire experiment, which includes the combination of endothermic and exothermic processes) results in an expression for the total specific heat release, $Q = \int q(T)\, dt$, which in turn is equal to $-\Delta H$ (where ΔH is the change in enthalpy of a chemical reaction).[9] One can then compare the measured change in enthalpy to calculated values, which are derived from the set of possible overall chemical reactions (i.e., as obtained from the literature). The relevant chemical reaction is assumed to be that reaction with a calculated value of ΔH similar to the measured value.

D. Analysis Protocol using the Direct-Heating Approach

For the direct-heating approach, the different heating regimes described earlier, and illustrated by Fig. 3B, can be characterized by Eq. 1. Initially, the sample is heated to a prescribed steady-state temperature with the heating beam (Regime 1 in Fig. 3B). At the steady-state temperature (end of Regime 1), the probe beam is directed onto the sample, causing the sample temperature to rise slightly to a new steady-state temperature (Regime 2). The probe beam is then blocked so that the sample temperature decays to the original steady-state temperature (Regime 3,

passive system response). Note that this approach is used for non-reacting substances or residue remaining after completion of chemical reactions (as indicated in Fig. 3B). Specifically, the two regimes corresponding to the perturbed sample temperature (i.e., Regimes 2 and 3 in Fig. 3B, respectively) are expressed by:

Temperature Rise: $$m\,c_p(T)\,(dT/dt)_{Reg2} = (I_I A)_{pb}\,\beta(T,\lambda) - F(T,T_o) \tag{8}$$

Steady State: $$(I_I A)_{pb}\,\beta(T,\lambda) = F(T,T_o) \tag{9}$$

Temperature Decay: $$m\,c_p(T)\,(dT/dt)_{Reg3} = -F(T,T_o) \tag{10}$$

where the subscript *pb* refers to the probe beam (i.e., with the heating beam still maintaining the steady-state temperature T_o). The relaxation time, τ^*, is determined from Regime 3, using Eq. 3,

$$\frac{dT}{dt} = -\frac{(T - T_o)_{Reg3}}{\tau^*} \tag{11}$$

E. Determining Substance Absorptivity

The substance absorptivity, $\beta(T,\lambda)$, is determined by evaluating Eqs. 9 and 10. Regression analysis of the measured sample thermogram is used to fit the best exponentially decaying expression to the data, which then provides an estimate of the three expression fitting parameters, i.e., τ^*, T_o, and T_{max}. To evaluate the absorptivity, Eq. 10 is substituted into Eq. 9 through the term $F(T, T_o)$, which represents the intersection of both the perturbed steady state and decay regimes. The temperature derivative dT/dt in Eq. 11 is then determined for Regime 3. This derivative is evaluated at the intercept of the thermogram temperature at $t = 0$ in Regime 3, i.e., for $T = T_{max}$ (viz., $[dT/dt]^{Tmax}$). The sample mass is determined using a commercial precision mass balance (with resolution of 1×10^{-5} g), and the value of the specific heat capacity is calculated at T_{max}. The value of $c_p(T_{max})$ is based on taking the weighted mean (if the sample is multicomponent or sitting on a substrate) from exponential expressions of $c_p(T)$ (i.e., regressive fits of the data found in Haynes et al.[13] One can then evaluate the heat transfer term, $F(T,T_o)$, at T_{max} with Eq. 10. It then follows from Eq. 9 that the term $\beta(T,\lambda)$ at both T_{max} and λ can be determined after estimating the probe-beam laser power.

F. Particle Absorption Based on Conservation of Electromagnetic Radiation

For an individual particle, absorption is normally evaluated in terms of the absorption cross section, C_{abs}.[14] This calculation can be accomplished using a modified version of Eq. 1, for which the absorptivity term is replaced by the absorption efficiency, Q_{abs} (= $C_{abs}/\pi d^2$). For an ensemble of particles (e.g., aerosol), Beer's Law[14] is used to obtain the absorption coefficient, α, which is dependent on the characteristic path length (d_c) through the aerosol. For particles on or within a substrate (e.g., a particle-laden filter), determination of the particle absorption coefficient is somewhat more complex. The analysis is dependent on the conservation of incident radiation at a surface (see Presser[10]), and is expressed as:

$$\rho + \tau + \beta = 1 \tag{12}$$

where ρ is the sample reflectivity (surface phenomenon including both specular and diffuse components), τ is the sample transmissivity (including specular and diffuse components), and β is the sample absorptivity (near surface phenomenon for opaque substances.[15] If ρ is the fraction of incident radiation intensity that is reflected, then it follows[14]:

$$\rho = I_\rho / I_I \tag{13}$$

$$\tau = I_\tau / I_I = (1-\rho)^2 e^{-\alpha d_c} \tag{14}$$

and from Eq. 12:

$$\beta = I_\beta / I_I = 1 - \rho - (1-\rho)^2 e^{-\alpha d_c} \tag{15}$$

where I_ρ is the reflected intensity, I_τ is the transmitted intensity, and I_β is the resulting intensity absorbed by the sample, ε is the extinction coefficient ($\varepsilon \equiv \alpha + \sigma$]),[14,16] and σ is the scattering coefficient.

G. Particle Absorption Coefficient for Particle-Laden Substrates

The protocol for determining the absorption coefficient of a particle-laden substrate also requires estimating values for ρ and ε. Thus for closure, in addition to measurement of the absorptivity (as described above), the transmissivity is also determined using a classical arrangement (see Fig. 4 and Eq. 14).[14] With measurements for both β and τ, the reflectivity is determined from Eq. 12, and the extinction coefficient is determine from

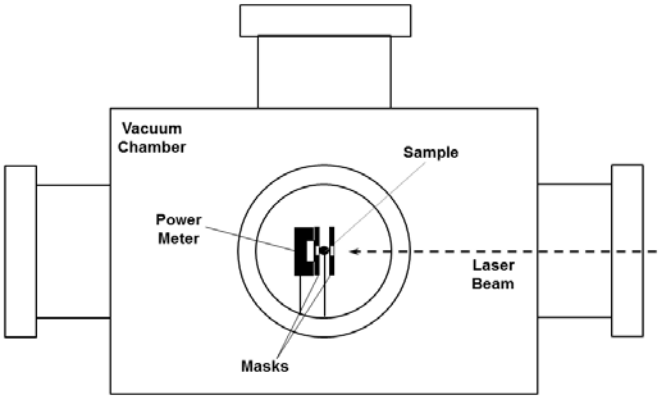

Figure 4. Schematic of the optical arrangement for measuring sample transmissivity.

$$\varepsilon = -\frac{1}{d_c}\ln\left[\frac{\tau}{(1-\rho)^2}\right] = -\frac{1}{d_c}\ln\left[\frac{1-\rho-\beta}{(1-\rho)^2}\right] \tag{16}$$

for $\tau, \beta, \rho > 0$.

If the scattering coefficient is negligible (i.e., for absorbing samples) then $\varepsilon = \alpha$.

Measurement from both the particle-laden filter and a clean filter enables one to isolate the particle characteristics. To obtain the particle absorption coefficient for a substrate laden with absorbing particles (i.e., without the filter contribution), one can use the following relationships:

$$\beta_{ps} = \beta_p + \beta_s \tag{17}$$

and

$$\tau_{ps} = \tau_p \cdot \tau_s = e^{-A^*_{ps}} = e^{-(A^*_p + A^*_s)} \tag{18}$$

where A^* is the absorbance ($A^*_i = \varepsilon_i\, d = -\ln(\tau_i)$, $i = p, s$), and the subscripts *ps*, *s* and *p* refer to the particle-laden substrate, clean substrate, and isolated particles, respectively.

H. Particle Mass-Specific Absorption Cross Section

Sample absorbance, A^*, is often reported on a mass specific basis (e.g., Weingartner et al.[17]), such that $A^* = C\,M = C\,\rho_p\,d_c$, where C is the mass-specific absorption cross section [$m^2 \cdot g^{-1}$], M is the particle mass loading (= m/A) [$g \cdot m^{-2}$], and ρ_p is the mass density (concentration) [$g \cdot m^{-3}$]. The mass-specific absorption cross section can be then written as $C = \alpha\, d_c / M = \alpha\, d_c\, A/m$.

IV. Past and Current Applications of the LDTR Technique

The LDTR heating-rate and direct-heating approaches have been applied to several different investigations. The summary given below demonstrates the applicability of the technique.

A. Hazardous Waste Safety

Energetic hazardous wastes are composed of a complex multiphase mixture of organics, solvents, additives, and a variety of other inorganic substances.[18] Determination of the potential for release of such wastes to the environment, as caused by a rapid release of chemical energy, is a difficult and complex problem. Such a release can be caused by several factors, such as a thermally accelerating runaway reaction, and/or high-energy initiator (e.g., lightning or fire). How such waste mixtures behave and react during exposure to a high-energy initiator, and what are the chemical reaction byproducts, can be of great concern. The behavior of these substances can be dependent on many parameters, including the substance physical and chemical properties, as well as the properties of the surrounding environment.

The total heating value and heat release rate of waste exothermal processes can act as a means to characterize the tendency for uncontrolled reactions (e.g., thermally explosive reactions). A simulant high-level organic waste (referred to as PAS 94) was used to demonstrate the energy release/absorption processes that may be involved with such substances.[9] This simulant consisted of over 24 different compounds including organics, inorganics, solvents, sodium nitrate, sodium nitrite, and additives. Five compounds comprised about 67 % of the total mixture (i.e., 31.48 % NaOH, 15.40 % $NaNO_3$, 7.39 % $NaNO_2$, 7.10 % $NaC_2H_3O_3$, and 6.3 % H_2O).

The LDTR and a DSC were used to study the behavior of PAS 94. Using the LDTR heating-rate approach, the dependence of sample temperature with time was investigated for pre-dried (in a vacuum oven at room temperature for two days) and undried sample. Figure 5 presents the sample temperature (Fig. 5A) and temperature difference Fig. 5B) with respect to time for undried PAS 94. Figure 5A presents heating curves for both the baseline (i.e., heating of the substrate without sample) and sample (i.e., sample with the substrate). The arrows indicate the presence of an accelerated rate of heat release at about 25 s (i.e., exothermic reaction). The dashed line is a curve fit to the data prior to the accelerated heat release at 25 s to indicate how the data might evolve at higher sample temperatures if the process remained endothermic. The energy released (exothermic) or absorbed (endothermic) by the sample with time is function of the temperature difference between the sample and baseline, as presented in Fig. 5B for the undried simulant waste PAS 94. One can solve Eq. 1 using the temperature difference given in Fig. 5B to obtain the specific heat release rate due to chemical reaction, $q(T)$ (with $q(T) < 0$ representing an endotherm and $q(T) > 0$ representing an exotherm). Comparing results in Fig. 5, the undried waste was endothermic between 440 K and 735 K and exothermic between 735 K and 910 K.

Differential scanning calorimetry (with a heating rate of 5 K/min) results with undried sample indicated that at temperatures between 300 K and 450 K there was a strong endotherm of about 731 J/g, an exotherm at 500 K to 650 K of about 654 J/g, and another exotherm at 730 K to 780K of about 5.8 J/g; with a net absorbed energy of about 71 J/g. The measurement expanded uncertainty is estimated to be within 2 %. Sample pre-drying caused the exothermal energy release between 500 K and 650 K to decrease from 654 J/g to 359 J/g. The endotherm between 300 K and 450 K decreased significantly from 731 J/g to 76 J/g, and the exotherm between 730 K and 780 K increased from 5.8 J/g to 84 J/g. As a result, the net energy release increased to 367 J/g, which was attributed to a decrease in evaporation of water.

For the LDTR (with heating rates of between 30 K/s to 40 K/s), results for the undried sample indicated that endothermic processes dominated the early stage of heating in the sample temperature range of 440 K to 630 K (where the heating curve for the sample is below the baseline in Fig. 5A). Exothermic processes dominated the later stages of heating in the sample temperature range of 735 K to 910 K (where the heating curve is above the baseline in Fig. 5A). Presumably, the accelerated rate of heat release at 25 s (not apparent with the DSC) was attributed to completion of the endothermic process and initiation of an exothermic process. Thus, assuming a two-stage process, the total endothermic specific heat release of the undried sample for the lower temperature range (defined as Stage A) was -1.2 kJ/g. The measurement expanded uncertainty is estimated to be within 10 %. The total exothermic specific heat release for the higher temperature range (defined as Stage B) was 2.9 kJ/g. The total heating value of the undried sample (i.e., endotherm and exotherm together) was 1.7 kJ/g. In the case of the pre-dried sample, the results appeared to be quantitatively similar. These results suggest that the thermal release characteristics of PAS 94 waste may not depend only on combustion of organics in oxygen.

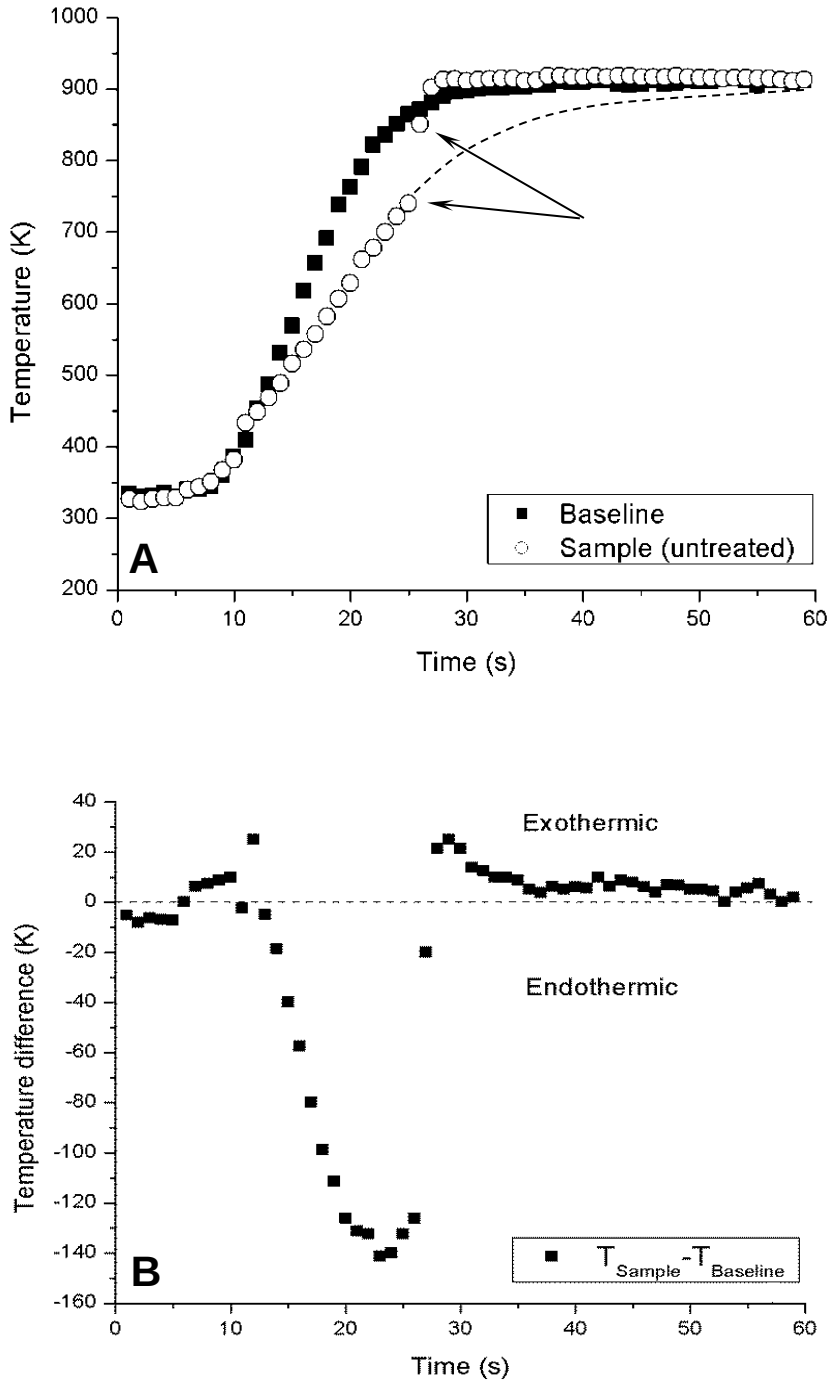

Figure 5. Variation of the sample A) temperature and B) temperature difference (between the sample and baseline) with time for the undried simulant waste PAS 94. The arrows indicate the presence of an accelerated rate of heat release. The dashed line is a curve fit to indicate how the data might evolve if the process remained endothermic.

B. Forensics of Homemade Explosives

Synthesized homemade explosive (HME) materials have been and continue to be used by extremists and terrorists due to the widespread availability and easy accessibility of the precursors. This is a major concern expressed by the Federal Government[19] with regard to improvised explosive devices of which HMEs are an essential component. Accurate forensic information on HMEs is critical for identifying the origin of the explosive materials and precursors, and determining HME formulation and synthesis procedures. Current forensic examination of the pre- and post-blast physical evidence lacks specificity for HME identification. Development of a thermal-/chemical-signature database, obtained for pre-selected HME precursor materials, would assist in forensic processing and analysis of data recovered from HME target locations (i.e., pre- and post-blast sites).

Homemade explosives are often composed of mixtures of both solid oxidizer and liquid fuel. The oxidation of the fuel is heterogeneous, and the rate of reaction depends on the contact surface area between the fuel and oxidizer. It has been documented (e.g., Rostberg[20]) that porous solids are often ground into powders to increase surface area and improve the total exothermic energy release. Porous surfaces can be thought of containing both an internal surface (i.e., network of pores) and external outer surface. The large internal solid surface absorbs, retains, and augments oxidizer contact area with the liquid fuel. Vaporization and dripping occur more readily on the external surface. Thus, oxidizer porosity and particle size are critical parameters for promoting exothermic chemical reactions.

Two of the more commonly used HME materials are ammonium nitrate (AN) and nitromethane (NM). The thermal behavior of AN is important from both an industrial and national security perspective. Ammonium nitrate is used in agriculture as a nitrogen fertilizer, and industry as an explosive material.[21] As a national security issue, extremists commonly use AN to manufacture HME.

To this end, experiments were carried out using the LDTR heating-rate approach[11] to study the thermal decomposition of NM and AN. In general, NM is an additive to AN; however, results for isolated NM and AN can be useful for evaluating mixture thermal degradation. The thermal energy release and chemical kinetics information were obtained for both substances at different temperatures, sample masses, and heating rates. Analyses were carried out to identify HME thermal behavior, i.e., exothermic and endothermic processes. The endothermic behavior is assumed to be attributed to organics (if present), water vaporization, phase transition, and/or chemical/thermal decomposition, while exothermic behavior is attributed to the occurrence of chemical reactions and possibly the presence of accelerated rates of thermal energy release (that may be indicative of uncontrolled reaction rates due to the energetic nature of the material).

Results indicated that the liquid-fuel saturation of the solid internal pores appears to be a limiting parameter for the total specific heat release during exothermic processes. The contribution of the external-surface liquid fuel to the total specific heat release is negligible during thermal oxidation and vaporization due to the relatively quick liquid mass change. For this study, results indicated a dependency of the AN thermal signatures on sample mass and laser heating rate, which was undetectable by other commercially available thermal analysis techniques (e.g., DSC and TGA). Figure 6 presents a typical ammonium nitrate thermal signature from the LDTR and a conventional differential thermal analyzer (DTA).[22] The LDTR heating rate was about 200 times faster than that of the DTA, which resulted in a much stronger signal with respect to time. The LDTR results also denote clearly important thermal-related features for AN, such as the melting, boiling, and thermal decomposition temperatures. Furthermore, the slower heating rate of the commercial instrument resulted in depletion of the sample (due to boiling and evaporation) before reaching the threshold temperature of the exothermic process.

C. Biomass Decomposition

Technologies for biomass-to-energy conversion are based on thermal, biochemical, and physical processing.[23] Fermentation is one commonly used conversion technique but is relatively slow and requires the integrated pretreatment of lignocellulose by enzymes, hydrolysis, or thermochemical processes for decomposition to simpler sugars.[24] Thermal conversion consists of either direct conversion of biomass to heat, steam, and electricity, or indirect conversion to energy carriers, such as bio-oil and bio-gas. Thermochemical conversion of biomass to biofuel is a complex process generally involving gasification and pyrolysis.[25] However, there is a basic lack of understanding of how chemical and thermophysical properties of biomass stocks relate to biofuel composition.[26]

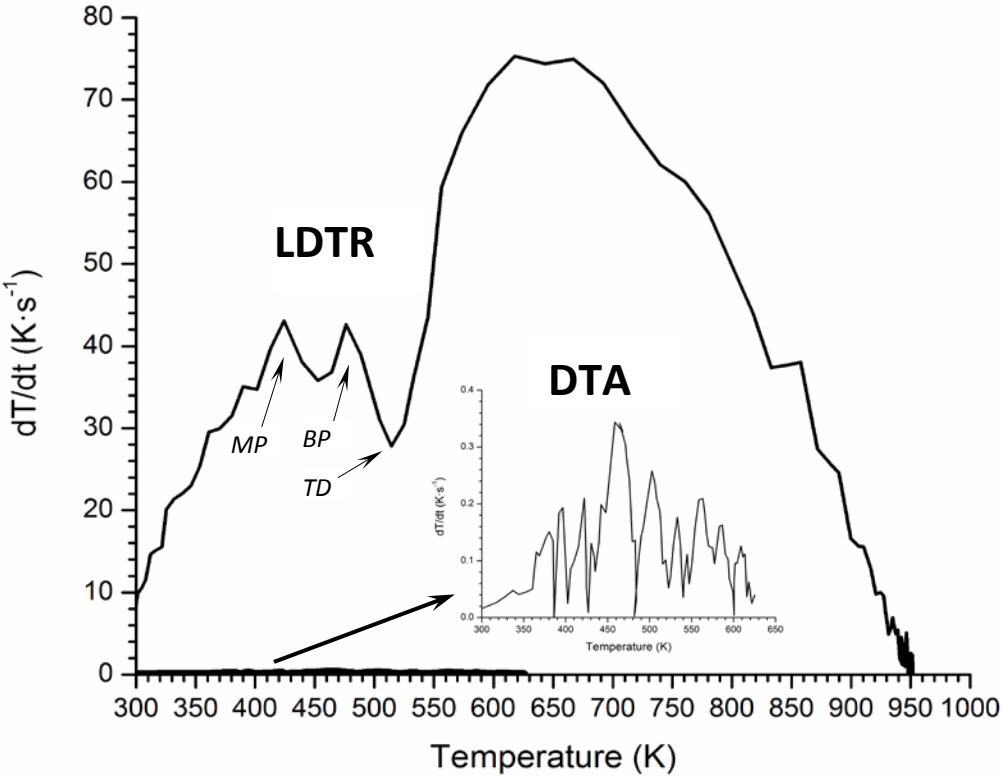

Figure 6. Typical ammonium nitrate (AN) thermal signature from the LDTR and a conventional differential thermal-analysis (DTA) technique.

For example, thermal oxidation of sugars within lignocellulose can lead to the formation of tars (caramelization) at temperatures between 400 K and 500 K,[27] which may clog passages (as those leading to automotive and aircraft engines). What is known about the caramelization process is that water is removed from a sugar (dehydration), proceeding to isomerization, fragmentation, and polymerization of the sugar into various high-weight compounds. Fragmentation reactions result in low-molecular-weight compounds which may be volatile, while polymerization reactions lead to larger molecular weight compounds, which contribute to the sugar dark brown color. Due to the lack of more detailed reaction information, thermochemical properties, and chemical reaction data are needed for different biomass properties and operating environments to assist in improving process conversion efficiency, as well as our understanding of the decomposition process.

One major issue with biomass-to-fuel conversion is the unknown chemical pathways involved in the decomposition of lignocellolose (i.e., plant cell wall composed of lignin, cellulose, and hemicellulose) directly to glucose.[28] To this end, the LDTR is currently being used with the direct-heating approach to investigate the caramelization of sucrose. In addition to LDTR thermochemistry results, reaction gas byproducts are collected and analyzed for chemical species identification. For the protocol presented in Fig. 3B, the sample is heated to the steady-state temperature with the assumption that chemical reactions occur during the heating up process to steady state. At steady state, the emitted gas byproducts are collected for analysis by a gas chromatography/mass spectrometer (GC/MS), see Fig. 2. Then the probe beam is initiated for the thermal analysis segment of the experiment. For the chemical byproduct analysis, peak identification of the most likely species was performed with the aide of the NIST automated mass spectral deconvolution and identification system (AMDIS) software to deconvolute the mass spectra.[29] An example is presented in Fig. 7, which was obtained for sucrose in nitrogen at 623 K, indicating a large peak for CO_2 and many additional smaller peaks to be identified. With the combination of the LDTR thermal analysis of the total heat release (i.e., change in enthalpy), and the additional chemical species information from the GC/MS, more analysis can be carried out to elucidate the possible chemical pathways associated with the decomposition of complex sugars.

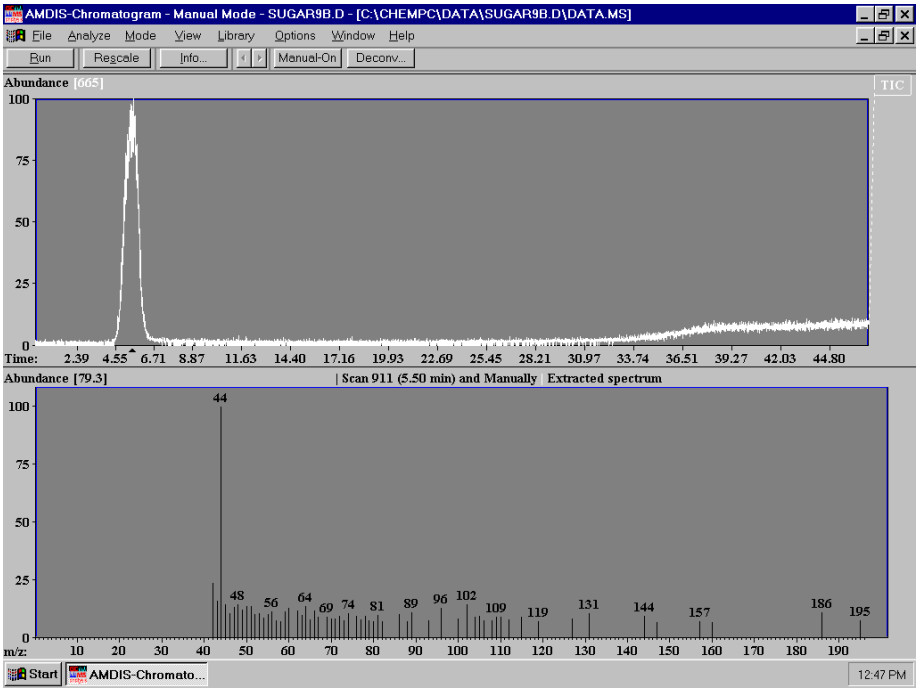

Figure 7. Typical GC/MS spectrograph of caramelized sucrose in nitrogen at 623 K.

D. Particle Absorption Characteristics for Atmospheric Aerosols

Collecting particles on filters is the most widely used technique for atmospheric aerosol sampling, primarily because of its low cost and simplicity.[30] Filter-based particle absorption techniques include the Aethalometer, (e.g., Hansen et al.[31]), integrating-plate/integrating-sphere photometer (e.g., Lawless et al.[32]), particle soot absorption photometer, PSAP (e.g., Bond et al.[33]), and continuous soot monitoring system, COSMOS (e.g., Kondo et al.[34], Nakasawa et al.[35]). The multi-angle absorption photometers, MAAP (e.g.,) was developed more recently, using radiative transfer considerations to compensate for filter surface reflected light (e.g., Moteki et al.[36], Collaud Coen et al.[37]), however, there still remain particle-loading limitations. These techniques are based on measuring the light transmission through the particle-laden filter to obtain the absorption coefficient from the Beer-Lambert law.

One important issue that has been reported extensively in the literature (e.g., Virkkula et al.[38], Taha et al.[39], Cappa et al.[40]) is filter substrate effects on determining the correct value for the particle absorption coefficient, often referred to as 'absorption enhancement'. This effect is attributed to absorption of backscattered laser light from the filter material, which on first pass is not absorbed by the particles discretely distributed over and embedded within the filter.[33, 41] As a result, a substantial increase may occur in the measured particle absorption.

In addition, an opposing effect to absorption enhancement is 'shadowing,' in which a heavier filter mass loading of absorbing particles on a filter surface results in an apparent diminished optical path length and concomitant reduction in the absorption coefficient.[17,42] Also, multiple-scattering effects for absorbing particles embedded within a fibrous filter appear to be obscured by the layer of surface particles, resulting in a similar decrease in absorption coefficient.[43,44] Thus, it is unknown to what extent absorption enhancement and shadowing effects influence the aerosol absorption properties.[45]

The LDTR was used with the direct-heating approach to determine the absorptivity of quartz-fiber (fibrous), Teflon (matted), and polycarbonate (membrane) filters coated with nigrosin (a highly absorbing dye[46]) over a range of steady-state temperatures.[10] Chemical reactions were not considered as nigrosin is nonreactive. Transmissivity measurements were also performed to provide the particle absorption coefficient and mass-specific cross section.[14] Measurements for both clean and coated filters enabled determination of the isolated particle absorption characteristics, which (when compared with the coated filters) was used to estimate absorption enhancement effects, as defined by

$$\alpha_R \equiv \frac{\alpha_{ps}}{\alpha_p} = \frac{C_{ps}\, m_{ps}}{C_p\, m_p}\,, \tag{19}$$

where C is the mass-specific absorption cross section, m is the sample mass, and the subscripts p and s refer to the particle and substrate (i.e., the filters), respectively. The variation of the sample absorption enhancement ratio with steady-state temperature was determined for the different filter materials and mass loadings, e.g., see Figs. 8. The results indicate that the value of α_R increases as the mass loading decreases and as the value of T_o increases. The effects of the filter substrate on enhancing absorption tends to be more significant for increasing steady-state temperature, lighter mass loadings, and for filter substrates with smaller pore sizes. The values of the absorption enhancement ratio for the polycarbonate filters compared well with values found in the literature[17,39,47].

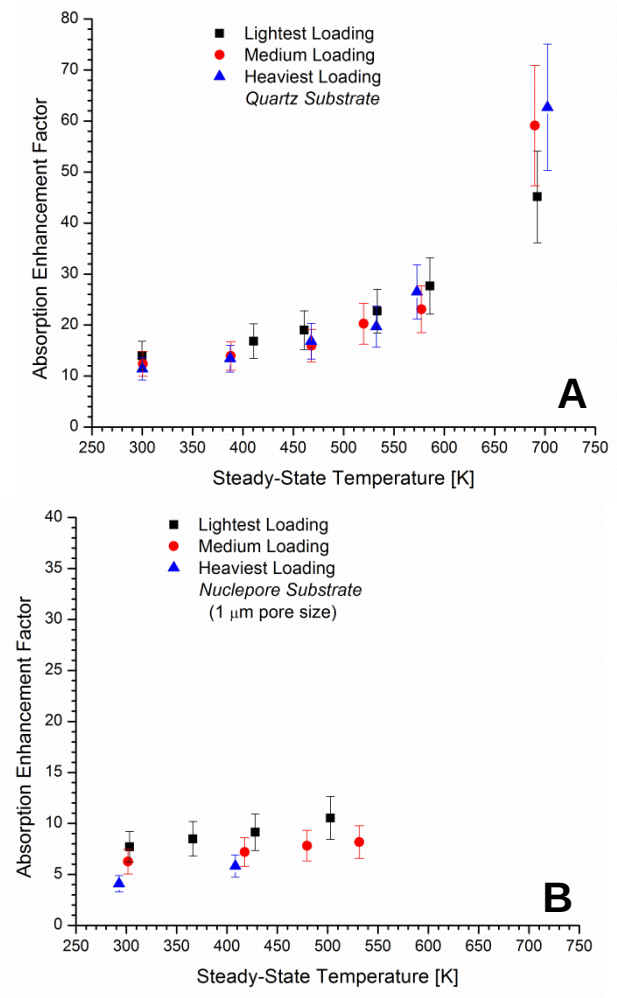

Figure 8. Variation of nigrosin absorption enhancement factor with steady-state sample temperature at different particle mass loadings for A) quartz and B) Nuclepore (1 μm pore size) substrates.

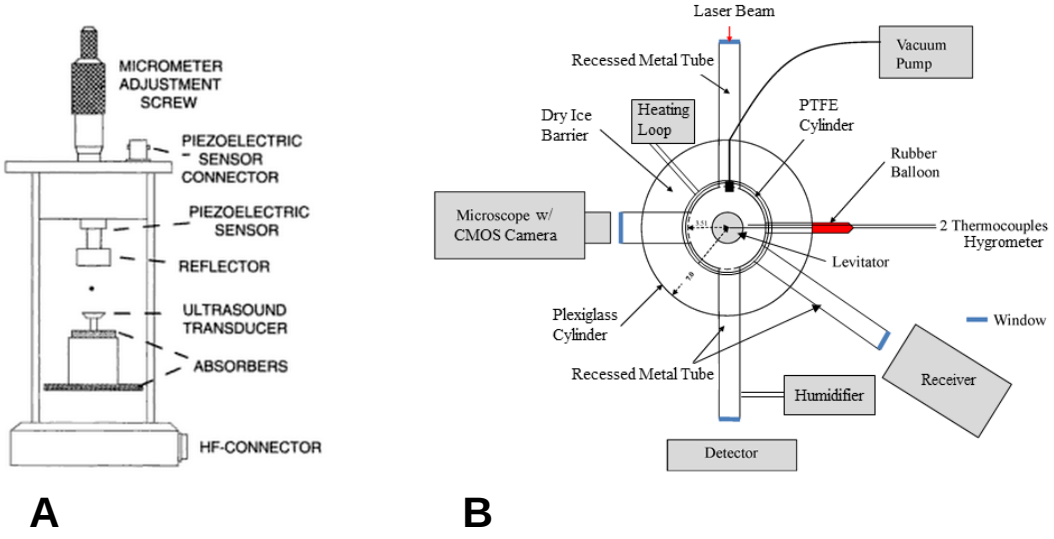

Figure 9. Schematic of A) acoustic levitator and B) surrounding diagnostic equipment for obtaining the optical characteristics of isolated frozen droplets and ice crystals.

E. Ice Crystal Absorption Cross Sections

One major source of aerosol emissions in the atmosphere is from aircraft exhaust. Soot immersed in or attached to contrail ice particles may increase the absorption of solar radiation, thus reducing the albedo of contrails.[48] One of the weaknesses of radiative forcing calculations is that light-absorbing aerosols are not fully treated, i.e., both direct and indirect effects, in part because absorbing aerosols are perhaps the most difficult substances to infer climate temperature change.[49] Furthermore, the chemical effects of black carbon and sulfate particles on the microphysical properties (e.g., the refractive indexes) of ice particles in cirrus clouds in the upper troposphere/lower stratosphere (UTLS) are poorly known and need to be improved.[50] Numerical studies have demonstrated the potential effect of soot on formation of ice particles and cirrus clouds but its effect has not been quantified,[51, 52] although the radiative forcing effect is thought to be positive.[53]

Sulfur also enhances absorption characteristics of soot particles, alters the chemical reactivity of dry soot, and provides volatile solid precursors for ice nucleation and growth.[54,55] A clear correlation between fuel sulfur content and soluble mass fractions found on fresh exhaust soot suggests that soot hydrates more effectively with increasing sulfur content (sulfuric acid being the primary soluble constituent).[56] The interaction between sulfuric acid, water vapor, and soot in the UTLS has been observed to have a substantial impact on aerosol optical properties and cloud-forming processes.[57]

The measurement of the absorption cross section of water/sulfuric acid droplets with internally-mixed soot is to be carried out using a modified version of the LDTR direct-heating approach. However, the probe beam will be used to perturb subzero steady-state temperatures. Simulated atmospheric droplets will be introduced into an enclosed acoustic levitator (see Fig. 9) at near tropospheric conditions (e.g., pressure, temperature, humidity, and gas composition). Fine-wire thermocouples and nonintrusive optical techniques (e.g., optical pyrometry) are being used to monitor particle temperature signature. A long-distance microscope in conjunction with a macro-lens and CMOS camera is used to visualize and document the particle/droplet macro morphological features and temporal changes. Effects to be investigated include temporal life-cycle changes in absorption characteristics under different conditions (i.e., during droplet freezing, ice crystal nucleation and growth, chemical reaction, and droplet/crystal aging).

V. Summary

Results have been presented on the application of a novel laser-heating technique to measure thermochemical properties of a variety of substances. The technique is based on measurement of the substance thermal history and the theoretical analysis for thermal energy conservation. The processes investigated included the total energy

release of simulant hazardous waste energetic materials, thermal behavior of homemade explosive materials, and the absorption characteristics of different filter materials coated with absorbing particles. Current projects are focusing on analysis of sugar caramelization chemistry, and measurement of the absorption cross section of levitated particle-laden droplets under tropospheric conditions.

References

[1]Lewis, R.G., (ed.), *Hawley's Condensed Chemical Dictionary*, 1993, p. 1063.

[2]Carranza, J.E., Fisher, B.T., Yoder, G.D., Hahn, D.W., "On Line Analysis of Ambient Air Aerosols using Laser Induced Breakdown Spectroscopy," *Spectrochimica Acta Part B*, 2001, 56:851-864.

[3]Rodolfa, K.T., and Cremers, D., "Capabilities of Surface Composition Analysis using a Long Laser Induced Breakdown Spectroscopy Spark," *Appl. Spectrosc.*, 2004, 58(4):367-375.

[4]Witze, P.O., "High Energy Laser Diagnostics for Real Time Measurements of Diesel Particulate Matter Emissions, *Proc. 7th Int. Congr. Optical Particle Characterization*, Kyoto, Japan, 2004.

[5]Melton, L.A., "Soot Diagnostics Based on Laser Heating," *Appl. Opt.*, 1984, 23(13):2201-2208.

[6]Kruger, V., Wahl, C., Hadef, R., Geigle, K.P., Stricker, W., and Aigner, M., "Comparison of Laser Induced Incandescence Method with Scanning Mobility Particle Sizer Technique: the Influence of Probe Sampling and Laser Heating on Soot Particle Size Distribution," *Meas. Sci. Technol.*, 2005, 16:1477-1486.

[7]Zhuravlev, E., and Schick, C., "Fast Scanning Power Compensated Differential Scanning Nano-Calorimeter: 1. The Device, and 2. Heat Capacity Analysis," *Thermochimica Acta*, 2010, 505:1-21.

[8]Piekiel, N.W., Cavicchi, R.E., and Zachariah ,M.R., "Rapid-Heating of Energetic Materials using a Micro-Differential Scanning Calorimeter," *Thermochimica Acta*, 2011, 521:125-129.

[9]Nazarian, A., and Presser, C., "Thermal and Chemical Kinetic Characterization of Multiphase and Multicomponent Substances by Laser Heating," *Int. J. Heat Mass Transf.*, 2008, 51(5-6):1365-1378.

[10]Presser, C., "Absorption Coefficient Measurements of Particle-Laden Filters using Laser Heating: Validation with Nigrosin," *J. Quant. Spectrosc. Radiat. Transf.*, 2012, 113(8):607-623.

[11]Nazarian, A., and Presser, C., "Forensic Analysis Methodology for Thermal and Chemical Characterization of Homemade Explosives," *Thermochimica Acta*, 2014, in press.

[12]Taylor, B.N., and Kuyatt, C.E., "Guidelines for Evaluating and Expressing the Uncertainty of NIST Measurement Results," NIST Technical Note 1297, National Institute of Standards and Technology, Gaithersburg, MD, 1994.

[13]Haynes, W.M., et al., (ed.), *CRC Handbook of Chemistry and Physics*, 91st ed., CRC Press, Taylor and Francis, Boca Raton, FL, 2011, pp. 12-195 and 12-205.

[14]Bohren, C.F., and Huffman, D.R., *Absorption and Scattering of Light by Small Particles*, Wiley, New York, 1983, pp. 28-41, 77-81.

[15]Incropera, F.P., and DeWitt, D.P., *Introduction to Heat Transfer*, 4th ed., Wiley, New York, 2001, pp. 248, 516, and 662-663.

[16]Siegel, R., and Howell, J.R., *Thermal Radiation Heat Transfer*, 2nd ed., Hemisphere, New York, 1981, Chapters 13 and 19.

[17]Weingartner, E., Saathoff, H., Schnaiter, M., Streit, N., Bitnar, B., and Baltensperger, U., "Absorption of Light by Soot Particles: Determination of the Absorption Coefficient by Means of Aethalometers," *J. Aerosol Sci.*, 2003, 34(10):1445-1463.

[18]Scheele, R.D., Sell, R.L., Sobolik, J.L., and Burger, L.L., "Organic Tank Safety Project: Preliminary Results of Energetics and Thermal Behavior, Studies of Model Organic Nitrate and/or Nitrite Mixture and Simulated Organic Waste," PNL-10213/UC-721, 1995.

[19]The White House, "Policy Statement for Countering Improvised Explosive Devices," Washington, DC, 2013.

[20]Rostberg, J.I., "Common Chemicals as Precursors of Improvised Explosive Devices: The Challenges of Controlling Domestic Terrorism," Naval Postgraduate School Monterey, CA, 2005.

[21]Akhavan, J., *The Chemistry of Explosives*, 2 ed., R. Soc. Chem., Cambridge, United Kingdom, 2004, pp. 77-82.

[22]Kiiski, H., "Stabilization of Ammonium Nitrate and AN-Based Fertilizers," *Proc. Int'l Fertilizer Soc.*, 2006, Proc. 583.

[23]McKendry, P., "Energy Production from Biomass (Part 2): Conversion Technologies." *Bioresour. Technol.*, 2002, 83:47-54.

[24]Department of Energy, "Biomass Multiyear Program Plan," Office of the Biomass Program Energy Efficiency and Renewable Energy, May 2009.

[25]Foust, T.D., Aden, A., Dutta, A., and Phillips, S., "An Economic and Environmental Comparison of a Biochemical and a Thermochemical Lignocellulosic Ethanol Conversion Processes," *Cellulose*, 2009, 16:547-565.

[26]Huber, G.W., "Breaking the Chemical and Engineering Barriers to Lignocellulosic Biofuels: Next Generation Hydrocarbon Biorefineries," National Science Foundation, Chemical, Bioengineering, Environmental, and Transport Systems Div., Washington DC, 2008, 180:30-47.

[27]Haika, O., et al., "Characterizations of Self-Combustion Reactions (SCR) for the Production of Nanomaterials used as Advanced Cathodes in Li-Ion Batteries, *Thermochimica Acta*, 2009, 493:96-104.

[28]Jacoby, M., "Chemicals from the Garden," *Chem. Eng. News*, 2009, July Issue:26-28.

[29]Mallard, W.G., and Reed, J., "Automated Mass Spectral Deconvolution & Identification System-Version [2.1]," National Institute of Standards and Technology, Gaithersburg MD, 1997.

[30]Lodge, J.P., Jr., *Methods of Air Sampling and Analysis*, 3rd ed., Lewis Publishing, Michigan, 1989.

[31]Hansen, A.D.A., Rosen, H., and Novakov, T., "The Aethalometer - An Instrument for the Real-Time Measurement of Optical Absorption of Aerosol Particles," *Sci. Total Environ.*, 1984, 36:191-196.

[32]Lawless, P.A., Rodes, C.E., and Ensor, D.S., "Multiwavelength Absorbance of Filter Deposits for Determination of Environmental Tobacco Smoke and Black Carbon," *Atmos. Environ.*, 2004, 38(21):3373-3383.

[33]Bond, T.C., Anderson, T.L., and Campbell, D., "Calibration and Intercomparison of Filter-Based Measurements of Visible Light Absorption by Aerosols," *Aerosol Sci. Technol.*, 1999, 30(6):582-600.

[34]Kondo, Y., Sahu, L., Kuwata, M., Miyazaki, Y., Takegawa, N., Moteki, N., Imaru, J., Han, S., Nakayama, T., Oanh, N.T.K., Hu, M., Kim, Y.J., and Kita, K., "Stabilization of the Mass Absorption Cross Section of Black Carbon for Filter-Based Absorption Photometry by the use of a Heated Inlet," *Aerosol Sci. Technol.*, 2009, 43(8):741-756.

[35]Nakayama, T., Kondo, Y., Moteki, N., Sahu, L.K., Kinase, T., Kita, K., Matsumi, Y., "Size-Dependent Correction Factors for Absorption Measurements using Filter-Based Photometers: PSAP and COSMOS," *J. Aerosol Sci.*, 2010, 41(4):333-343.

[36]Moteki, N., Kondo, Y., Nakayama, T., Kita, K., Sahu, L.K., Ishigai, T., Kinase, T., and Matsumi, Y., "Radiative Transfer Modeling of Filter-Based Measurements of Light Absorption by Particles: Importance of Particle Size Dependent Penetration Depth," *J. Aerosol Sci.*, 2010, 41(4):401-412.

[37]Collaud Coen, M., Weingartner, E., Apituley, A., Ceburnis, D., Fierz-Schmidhauser, R., Flentje, H., Henzing, J.S., Jennings, S.G., Moerman, M., Petzold, A., Schmid, O., and Baltensperger, U., "Minimizing Light Absorption Measurement Artifacts of the Aethalometer: Evaluation of Five Correction Algorithms," *Atmos. Meas. Technol.*, 2010, 3(2):457-474.

[38]Virkkula, A., Ahlquist, N.C., Covert, D.S., Arnott, W.P., Sheridan, P.J., Quinn, P.K., and Coffman, D.J., "Modification, Calibration and a Field Test of an Instrument for Measuring Light Absorption by Particles," *Aerosol Sci. Technol.*, 2005 39(1):68-83.

[39]Taha, G., Box, G.P., Cohen, D.D., and Stelcer, E., "Black Carbon Measurement using Laser Integrating Plate Method," Aerosol *Sci. Technol.*, 2007, 41(3):266-276.

[40]Cappa, C.D., Lack, D.A., Burkholder, J.B., and Ravishankara, A.R., "Bias in Filter-Based Aerosol Light Absorption Measurements due to Organic Aerosol Loading: Evidence from Laboratory Measurements," *Aerosol Sci. Technol.*, 2008, 42(12):1022-1032.

[41]Clarke, A.D., "Effects of Filter Internal Reflection Coefficient on Light Absorption Measurements made using the Integrating Plate Method," *Appl. Opt.*, 1982, 21(16):3021-3031.

[42]Conny, J.M., Norris, G.A., Gould, T.R., "Factorial-Based Response-Surface Modeling with Confidence Intervals for Optimizing Thermal-Optical Transmission Analysis of Atmospheric Black Carbon," *Analytica Chimica Acta*, 2009, 635(2):144-156.

[43]Arnott, W.P., Hamasha, K., Moosmuller, H., Sheridan, P.J., Ogren, J.A., "Towards Aerosol Light Absorption Measurements with a 7-Wavelength Aethalometer: Evaluation with a Photoacoustic Instrument and a 3-Wavelength Nephelometer," *Aerosol Sci. Technol*., 2005, 39(1):17-29.

[44]Kirchstetter, T.W., and Novakov, T., "Controlled Generation of Black Carbon Particles from a Diffusion Flame and Applications in Evaluating Black Carbon Measurement Methods," *Atmos. Environ.*, 2007, 41(9):1874-1888.

[45]Baumgardner, D., et al., "Soot Reference Materials for Instrument Calibration and Intercomparisons: A Workshop Summary with Recommendations," *Atmos. Meas. Technol.*, 2012, 5(8):1869-1887.

[46]Sedlacek, A., and Lee, J., "Photothermal Interferometric Aerosol Absorption Spectrometry," *Aerosol Sci. Technol.*, 2007, 41(12):1089-1101.

[47]Bond, T.C., and Bergstrom, R.W., "Light Absorption by Carbonaceous Particles: An Investigative Review," *Aerosol Sci. Technol.*, 2006, 40(1):27-67.

[48]Noppel , F.G., "Contrail and Cirrus Cloud Avoidance Technology," Ph.D. Thesis, School of Mechanical Engineering, Cranfield University, Bedfordshire, United Kingdom, 2007.

[49]Wuebbles, D.J., Yang, J.H., and Herman, R., "Climate Metrics and Aviation: Analysis of Current Understanding and Uncertainties," ACCRI Subject specific white paper on metrics for climate impacts (SSWP #VIII), Aviation Climate Change Research Initiative, 2008.

[50]Yang, P., Dessler, A., and Hong, G., "Contrails/Cirrus Optics and Radiation," ACCRI Subject specific white paper on metrics for climate impacts (SSWP #VI), Aviation Climate Change Research Initiative, 2008.

[51]Hendricks, J., Kärcher, B., Döpelheuer, A., Feichter, J., Lohmann, U., and Baumgardner, D., "Simulating the Global Atmospheric Black Carbon Cycle: A Revisit to the Contribution of Aircraft Emissions," *Atmos. Chem. Phys.*, 2004, 4:2521-2541.

[52]Lohmann, U., Kärcher, B., and Hendricks, H., "Sensitivity Studies of Cirrus Clouds formed by Heterogenous Freezing in the ECHAM GCM," *J. Geophys Sci.*, 2004, 109:D1620, doi:10.1029/2003JD00443.

[53]Minnis, P., "Contrails, Cirrus Trends, and Climate," *J. Climate*, 2004, 17:1671-1685.

[54]Petzold, A., et al., "On the effects of Hydrocarbon and Sulphur-Containing Compounds on the CCN Activation of Combustion Particles," *Atmos. Chem. Phys. Discuss.*, 2005, 5(3):2599-2642.

[55]Schumann, U., Arnold, F., Busen, R., Curtius, J., Kärcher, B., Kiendler, A., Petzold, A., Schlager, H., Schröder, F., Wohlfrom, K.H., "Influence of Fuel Sulfur on the Composition of Aircraft Exhaust Plumes: The Experiments SULFUR 1-7," *J. Geophys. Res.*, 2002, 107(D15), doi/10.1029/2001JD00813.

[56]Kärcher, B., Busen, R., Petzold, A., Schröder, F.P., Schumann, U., and Jensen, E.J., "Physicochemistry of Aircraft-Generated Liquid Aerosols, Soot, and Ice Particles. 2. Comparison with Observations and Sensitivity Studies," *J. Geophys. Res.*, 1998, 103(D14):17129-17147.

[57]Khalizov, A.F., Zhang, R., Zhang, D., Xue, H., Pagels, J., and McMurry, P.H., "Formation of Highly Hygroscopic Soot Aerosols upon Internal Mixing with Sulfuric Acid Vapor," *J. Geophys. Res.*, 2009, 114:D05208, doi:10.1029/2008JD010595.